Opto-mechanisms design of extreme-ultraviolet camera onboard Chang E lunar lander

Zhaohui Li,* Bo Chen, Kefei Song, Xiaodong Wang, Shijie Liu, Liang Yang, Qinglong Hu, Ke Qiao, Liping Zhang, Guodong Wu, and Ping Yu

Changchun Institute of Optics, Fine Mechanics and Physics, Chinese Academy of Science, 130022, Dong Nanhu Road 3888, Changchun, China

lizh_ciom@aliyun.com

Abstract: The extreme-ultraviolet camera mounted on the Lander of China Chang-E lunar exploration project launched in 2013 is the first instrument used to imaging from the lunar surface to the whole plasmasphere around the earth. Taking into account both the lunar environment conditions and the weight and volume constraints, a single spherical mirror and a spherical microchannel plate detector make up the compact optical system. An optimized opto-mechanical design was presented using Finite Element Analysis Model, and the detail design for the important assemblies of the 2-axis platform, the primary mirror, the aperture door mechanism and MCP detector were all specially addressed for their environmental adaptability and reliability. Tests of mechanical characteristics have demonstrated that the position and pointing accuracy and its stability meets the operation requirements of 2′. Vibration results have shown that the EUVC has adequate stiffness and strength safety margin to survive in launch and the moon environments. The imaging performance with the resolution of 0.08° is measured after vibration, in agreement with the predicted performance.

OCIS codes: (120.0280) Remote sensing and sensors; (220.4880) Optomechanics; (120.4640) Optical instruments; (340.7480) X-rays, soft x-rays, extreme ultraviolet (EUV).

References and links

1. O. Y. Ziyuan, L. Chunlai, and Z. Yongliao, "The scientific object of the first phase project of Chinese lunar exploration," Spacecraft Eng. **14**(1), 1–5 (2005).
2. C. Bo and H. Fei, "Optical design of moon-based earth's plasmaspheric extreme ultraviolet imager," Opt. Precis. Eng. **19**(9), 2057–2062 (2011).
3. C. O. Davis, J. Bowles, R. A. Leathers, D. Korwan, T. V. Downes, W. A. Snyder, W. J. Rhea, W. Chen, J. Fisher, P. Bissett, and R. A. Reisse, "Ocean PHILLS hyperspectral imager: design, characterization, and calibration," Opt. Express **10**(4), 210–221 (2002).
4. J. H. Lee, C. W. Lee, Y.-M. Kim, and J.-W. Kim, "Optomechanical design of a compact imaging spectrometer for a microsatellite STSAT3," J. Opt. Soc. Korea **13**(2), 193–200 (2009).
5. G. R. Carruthers, "Apollo 16 far-ultraviolet camera/spectrograph: instrument and operations," Appl. Opt. **12**(10), 2501–2508 (1973).
6. P. Mouroulis, R. O. Green, and D. W. Wilson, "Optical design of a coastal ocean imaging spectrometer," Opt. Express **16**(12), 9087–9096 (2008).
7. M. G. Pelizzo, D. Gardiol, P. Nicolosi, A. Patelli, and V. Rigato, "Design, deposition, and characterization of multilayer coatings for the Ultraviolet and Visible-Light Coronagraphic Imager," Appl. Opt. **43**(13), 2661–2669 (2004).
8. L. Zhaohui, W. Zhongsu, H. Qinglong, and Y. Liang, "Design of tracking platform and analysis of its stiffness for lunar EUV camera," Chin. J. Sci. Instrum. **31**(10), 2352–2356 (2013).
9. C. M. Korendyke, C. M. Brown, R. J. Thomas, C. Keyser, J. Davila, R. Hagood, H. Hara, K. Heidemann, A. M. James, J. Lang, J. T. Mariska, J. Moser, R. Moye, S. Myers, B. J. Probyn, J. F. Seely, J. Shea, E. Shepler, and J. Tandy, "Optics and mechanisms for the Extreme-Ultraviolet Imaging Spectrometer on the Solar-B satellite," Appl. Opt. **45**(34), 8674–8688 (2006).
10. W W. A. Podgorski, D. Caldwell, K. McCracken, M. P. Ordway, P. N. Cheimets, K. Korreck, L. Golub, J. Cirtain, and K. Kobayashi, "Minimizing the mirror distortion for Subarcsecond imaging in the Hi-C EUV telescope," SPIE Proc. **8502**, 85020E1 (2012).
11. G. Murakami, K. Yoshioka, and I. Yoshikawa, "High-resolution imaging detector using five microchannel plates and a resistive anode encoder," Appl. Opt. **49**(16), 2985–2993 (2010).

#210949 - $15.00 USD Received 5 May 2014; revised 29 May 2014; accepted 16 Jun 2014; published 20 Jun 2014

12. J. P. Wülser, J. R. Lemena, and T. D. Tarbella, "EUVI: the STEREO-SECCHI extreme ultraviolet imager," SPIE Proc. **5171**, 111–122 (2004).
13. J. Mitsugi, K. Ando, Y. Senbokuya, and A. Meguro, "Deployment analysis of large space antenna using flexible multibody dynamics simulation," Acta Astronaut. **47**(1), 19–26 (2000).
14. L. Poletto, A. Boscolo, and G. Tondello, "Optical performances and characterization of an EUV and soft x-ray test facility," Proc. SPIE **3764**, 94–102 (1999).
15. D. S. Martínez-Galarce, A. B. Walker, D. B. Gore, C. C. Kankelborg, R. B. Hoover, T. W. Barbee, and P. F. Boerner, "High resolution imaging with multilayer telescopes: resolution performance of the MSSTA II Telescopes," Opt. Eng. **39**(4), 1063–1079 (2000).

1. Introduction

The extreme-ultraviolet camera (EUVC), as one of the important payloads in China lunar exploration project—Chang E Engineering, is being developed to image the Earth's plasmasphere from the lunar surface. It will observe the spatial structure and dynamics of the Earth's plasmasphere on a global scale, which plays an important role in complete the Chang E Engineering science objectives such as environmental monitoring, space weather forecasting and astronomy study. EUVC will detect the emission at 30.4nm and monitor changes of density and distribution of the Earth's plasmasphere with an operational duration of 1 year [1,2].

To successfully achieve the scientific observation goals for Chang E mission, EUVC need to meet the requirements with space extreme environments, vibration in launch, and strict constraints of volume and weight. So the EUVC will be a very compact instrument with a good space environmental adaptability. Here, the opto-mechanical design of EUVC and a demonstration of its validity through finite element analysis (FEA) as well as the imaging performance tests are presented [3].

2. Design specifications and optical system description

Imaging to the entire earth plasmasphere from the lunar surface requires the EUVC has the wide field of view and need be mounted on a two-dimension pointing and tracking platform to keep the EUVC to point to the earth by adjustment of 0.5°/day. So EUVC is composed of two parts: an extreme ultraviolet band imaging telescope and a two-axis gimbal platform. The main parameters and constraints for the EUVC related to optomechanical design are summarized in Table 1.

Table 1. Principle EUV design parameters

property	Value
Mass	16.5 kg
Power	20W
Size	470mm* 360mm*290mm
Field of view	15°
Optical design Prime focus	150mm
Angular resolution	0.1°
Sensitivity	0.1~0.2counts/s.Re
Eigenfrequencies	>70 Hz(in launch direction) >40 Hz(in lateral direction)
Operational lifetime	1 year in-orbit
Operational temperature	−50°C~ + 90°C-
Thermal interface	−140°C~ + 140°C
Larger vibration loads	Sine: 8g (5Hz~100Hz) Random: 10g (rms)

To respond the environmental challenges and design constraints of weight and volume, design-optomechanical efforts are focused on environmental adaptability design to achieve compact structure and to maintain the optical performance after launching, landing and the moon day/night recycle. The report gives the configuration, structure and mechanism design, selection of material, and system assembly method based on FEM simulating analysis [4,5].

For imaging optical system [6], two-mirror Cassegrain-type telescope has been studied in the planning of this instrument. But the optical configuration with a single spherical mirror

#210949 - $15.00 USD Received 5 May 2014; revised 29 May 2014; accepted 16 Jun 2014; published 20 Jun 2014

was finally chosen for the telescope to minimize the weight and volume. A multilayer-coated mirror is used as focusing EUV photons, a metal thin filter near the focal plane to suppress unwanted wavelength-longer emissions and microchanel plates with spherical surface to pick up photon events in the system [7]. In the fact, The Selenological and Engineering Explorer (SELENE) has used the similar type of optics. The optical schematic of the EUVC is shown in Fig. 1.

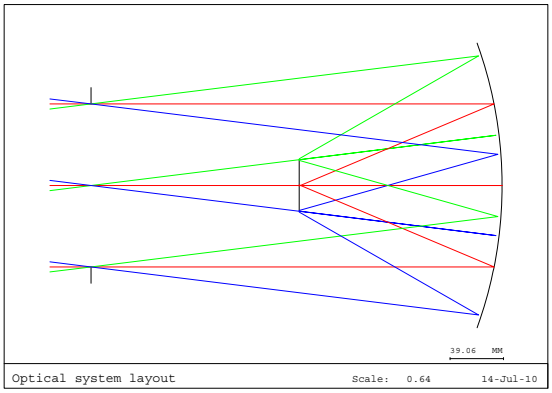

Fig. 1. Optical system of EUV camera.

The required angular resolution 0f 0.1° is achieved in the optical system over a 15° field of view with the minimum optical surface. The entrance pupil is located at the center of the spherical primary mirror for eliminating the effects of aberrations with 118mm aperture. Spot diagram is used to evaluate the optical system. The RMS spot diameter varies between 0.209 and 0.207 mm, respectively, for an on-axis object and, for the corners of the field of view, the spot size over the field of view is almost uniform. The position accuracy tolerance is reasonable by 0.05 mm mirror-detector separation error and 20″ slope error for image plane.

3. Two-axis platform mechanism

In the mechanical design process, EUVC has been benefited from the study of the several types of the aerial stable imaging platform, the previous tracking and the pointing mechanism design. According to general requirements of the lunar lander, the following design criteria should be fulfilled:

- The design is optimized for low mass and a minimum volume.
- Adequate stiffness and strength to survive during the launching and landing progress.
- The dimensional stability meets the requirements.
- The mechanism has the ability to be run in the extreme temperature environment.

There are basically two types of gimbals: Equatorial gimbals and azimuth/elevation gimbals. Despite equatorial type does not have keyhole problem near its zenith position, the disadvantages of large sweep volume and size are unacceptable in lunar exploration program. As a result, traditional Elevation/Azimuth two-axis platform is adopted which has the compromise merits in weight, small structure, and pointing accuracy. The details of the mechanical design, Finite Element Model (FEM) analysis and some tests to qualify the design have been done [8].

The two-axis platform holds the EUVC together with signal process electronics and high-voltage power supply module. To compensate the landing inclination of the lunar lander, the platform should have adequate range-of-motion with ± 45°elevation angle and ± 55° azimuthal angle. The pointing accuracies of the platform are 2′ around the azimuthal axis and around the elevation axis respectively. The platform consists of two separate modules:

#210949 - $15.00 USD Received 5 May 2014; revised 29 May 2014; accepted 16 Jun 2014; published 20 Jun 2014

elevation module and azimuth module, both modules are joined together via a U-shape support frame. The mechanical design must satisfy all strength and stiffness requirements, environment constraints and its interfaces with the lunar lander. The realized design is presented in Fig. 2.

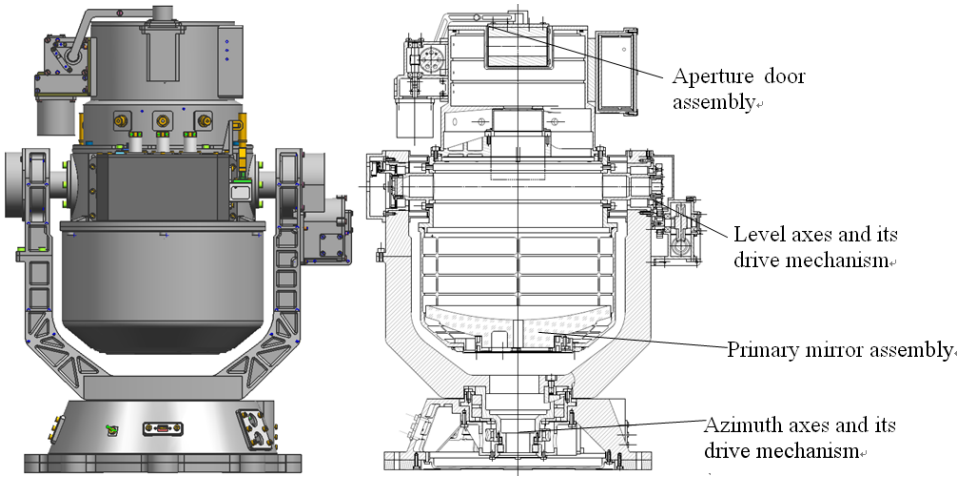

Fig. 2. The detail configuration and cross section of EUVC.

The elevation rotation module consists of the left and right level axis, stepper motor, gearbox to amplify the motor torque. Trade-off design between the sizes of bearing and its capabilities of vibration resistance are made based on dynamic analysis results. The duplex angular contact ball bearings with inner diameter of 25mm are utilized as main support of the level axis which determines the rigidity of the level axis, so it is preload reasonably to eliminate axial clearance. A single ball bearing which is preloaded by a flexible ring, is fixed on the other end of the level axis. The flexible ring should have the ability to compensate the thermal deformation of rolling bearings and the U-shape frame. Similarly, the azimuth axis module consists of a vertical axis, the duplex angular contact ball bearings with inner diameter of 75mm, and the supporter holding bearings [9].

The actuator module consists of a stepper motor, a worm-wheel box with speed ratio of 1:60 and two position sensors. Titanium has been used for the Actuator Module housing a box due to the reasons of low mass and CTE match with the other parts of the azimuth axis module. All the worm-wheels and bearings are dry lubricated by adhering to MoS_2. Using the self-clock property of worm gearing, it is able to maintain the position under high launch loads with an adequate safety margin. A high resolution stepper motor (1 °/step) with redundant windings has been developed for space application and optimized for maximum torque.

U-shape frame supports the imaging unit and electronic unit of the EUVC, which is one of the most important factors influencing mechanical characteristics of the 2-axis platform. The dynamic characteristics of the frame structures directly affect the adaptability of the system on vibrating environments. Different lightweight manners and several materials have been compared based on FEM model, Table 2 shows resonance frequency versus three kinds of materials. In the realistic instrument, U-shape frame is made of titanium for reasons of low mass and CTE match with level and azimuth axis which are also made of titanium.

Table 2. Natural frequencies of U-shape supporter structure

Materials	Vibration resonance frequency (Hz)		
	1st mode	2nd mode	3rd mode
Mg-alloy	245.43	262.47	443.71
Aluminum alloy	253.41	271.01	458.15
Titanium	318.36	338.36	573.86

#210949 - $15.00 USD Received 5 May 2014; revised 29 May 2014; accepted 16 Jun 2014; published 20 Jun 2014

The mass of the whole platform and imaging unit have been reduced as much as possible while still satisfying the required eigenfrequencies and maintaining adequate safety margins by structure FE-modeling analysis. On the other hand, the adaptability of the 2-axis platform in the lunar environment has been considered during design process and assembling phase. In order to reduce geometry deformation, all the structure elements have been kept in vacuum tube for 3 cycles from extreme cold −140°C to heat + 120°C, then the integrated 2-axis platform was processed using the same stress anneal technique.

4. EUV imaging telescope

The EUVC primary mirror is made of Zerodur, and its surface with roughness of 0.4nm is smooth very much, and finally is coated with a narrow pass band reflective MoSi multilayer, which is only optimized for the specific 30.4 nm emission while other emissions are excluded. Light reflected from the mirror is focused on the spherical focal surface of the sensor.

Noting the mirror structure shown in Fig. 3. The ring and radiation rubs are fabricated for light-weighted Zerodur on the rear surface of the mirror, and the center shaft from the back part of the mirror will be bonded to the mirror mount with suited gap. The mirror mount is made of Invar with near-zero CTE properties, which match the CTE of Zerodur. So the major strains will come from the procedure of assembling the mirror. Three flexure pads are fabricated around inner circular surface of the mirror mount to eliminate assemble strains, the center shaft of the mount is used to keep the mirror in the mount with normal position, being vertical to the bottom of the mirror mount. Meanwhile, the mirror centration is confined using thin shims between the mirror back shaft and the mirror mount. After adjustment, epoxy is injected into the bond gaps. In order to monitor the dynamic mirror thermal environment, a thermal sensor is bonded along the edge of a ring rub on the rear surface. As the thermal expansion coefficient of silica is lower ($1\sim3 \times 10^{-6}$/°C) than Titanium or Aluminum, the tube made of carbon fiber composite material is applied to keep the distance between the primary mirror and the spherical surface MCP detector changed in tolerance during the thermal cycling [10].

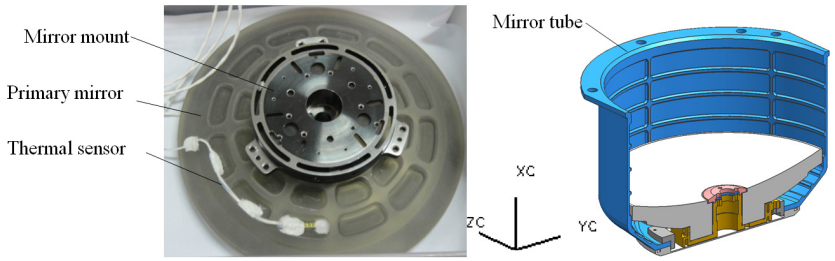

Fig. 3. The primary mirror assembly.

The changes of the mirror temperature is in the wide range of –45°C~ + 90°C, it is very stringent for the mirror assembly. Thermal analysis of the mirror assembly has been carried out with the temperature change of 70°C, the analysis results are shown in Table 3.

Table 3. Influence of temperature on figure

Variation of temperature	RMS value of figure	PV value of figure
△T = 70°C	13.44nm	71.03nm

As shown in Table 3, the figure accuracy of 13.44nm(λ/30) at wavelength of 632.8nm meets the requirements of optical image quality. To check for the thermal stress in the bonded mirror, interferometer measurements of the mirror after stored in the worst hot and cold conditions were taken at 20°C in clean room, and the deformation of the surface figure are within error budget allocation, nearly no change comparing with the measuring result in manufacture process.

#210949 - $15.00 USD Received 5 May 2014; revised 29 May 2014; accepted 16 Jun 2014; published 20 Jun 2014

5. MCP detector assembly

The detector is comprised of 3 curved-channel microchannel plate coated with photocathode layer, an anode plate is mounted at the back of the microchannel plate [11]. Detector housing consisting of ceramic and Kovar-rings welded to a stainless steel flange and window. The photocathode converts the incoming photons into photoelectrons. A high voltage applied across the MCP causes these photoelectrons to be accelerated through microchannels. The position in X-Y directions is determined by an electronics unit which includes preamplifiers and position-calculating circuitry. A schematic diagram of the MCP is shown in Fig. 4.

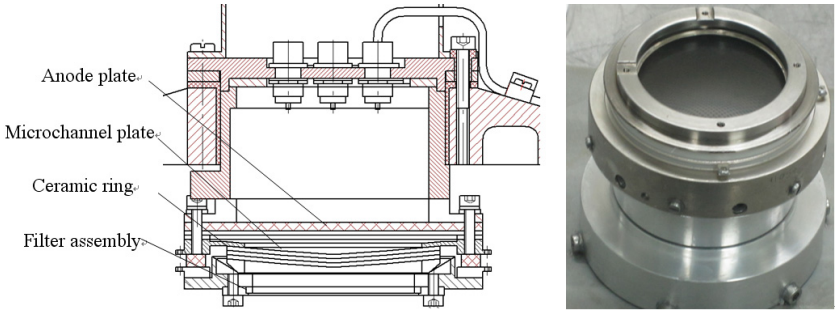

Fig. 4. Configuration of the MCP detector assembly.

The EUVC uses thin metal film filters in front of the detector to suppress undesired UV and the other radiation. The main damage to the filter is induced by air flow during launch, so the filter is protected by the aperture door to reduce the disturbance of airflow, and some small holes were manufactured on the filter mount. Air flow studies, combined with vibration analyses, followed by real tests were used to define venting holes (number, location, size).Besides the function to protect the fragile entrance filters during launch and landing process, the other primary function of the aperture door mechanism is used to be as the thermal control door [12]. Based on the thermal design, a heat radiator of Pu + 238 (Radiating heat Unit, RHU) was located on the aperture door. When the door closed in lunar night cycle, the RHU emitted heat to inner of the EUV camera, and remove the heat radiator when the door opened in lunar daytime. The door assembly is attached to the front aft of the lens tube, as shown in Fig. 2. The door is opened by a stepper motor and a self-lock worm wheel mechanism with 40:1 transmission rate.

6. Modeling analysis and mechanics performance

The design of the structure was studied with the help of a finite element model, predicting overall stiffness and strain levels. The 2-axis platform in the EUVC imaging system comprises of several rotation mechanism modules, and modeling the dynamic mechanism with clearance connections is a challengeable issue in true prediction of its mechanics performance. The gap element method is adopted instead of coupling point restriction method to address the problems on elasticity contact and gap joint. Finite element equations of the contact problem composed of gap elements have been described in the reference paper [13].

Based on gap element method, the elevation axis module and the azimuth axis module in the 2-axis platform system are described with elastic contact condition, the worm wheel gear drive modules are described with clearance condition, while the other structure such as U-shape support frame, etc are modeled using general point coupling theory. A FEM model has been realized by selecting solid-flexure unit and flexure-flexure unit in Patran analysis program, and the analysis results demonstrated that the design of EUVC system has adequate axial stiffness, which is of primary importance in the launch vibration environment, while the lateral direction eigenfrequencies is about 47Hz, larger than the minimum requested 40Hz

#210949 - $15.00 USD Received 5 May 2014; revised 29 May 2014; accepted 16 Jun 2014; published 20 Jun 2014

requested by satellite. Figure 5 shows the first 2 resonance modes in longitudinal direction and lateral direction respectively.

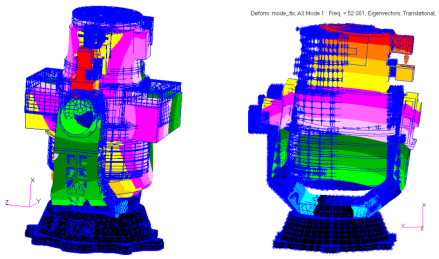

Fig. 5. Eigenfrequency of the 1st order mode shape based on gap element model. Left is vibration mode along launching direction, right is lateral direction with natural frequency of 47Hz.

Additionally, the vibration tests have been carried out to get rid of early invalidation. According to the sine scan test, the acquired 1st natural frequency is 42.8Hz, which is coincident to analysis result by FEM model. Therefore, the gap element model is proven to be able to truly describe the stiffness and strain level of the 2-axis tracking platform. After the severe vibration tests with sine input of 8g and random input of 10g(rms), the maximal stress occurring at the connection of level bearings and the U-frame is equal to 145MPa, which is safely below the proof stress of 440MPa. The structural design and stiffness safety margin meets the space experimental qualification requirements specified by the project of Chang E lunar exploration engineering.

7. Verification and imaging performance

Following the mechanical test, the EUVC were installed in vacuum chamber after assembly as an integrity instrument in order to relax connection strain and maintain size stability. Then begin thermal vacuum test which includes following measuring items: The functional and pointing performance (position accuracy, stability); Torque margin checks throughout the lifetime during temperature change; Imaging performance under all environmental conditions. The test system includes a EUV light source with stability of 5%(a hollow-cathode lamp filled with helium gas), a McPherson 247 monochromator, a collimator with focus length 750mm and a test chamber with vacuum of better than 1×10^{-4}Pa, and temperature changes between −140°C~ + 110°C.

In thermal vacuum tests, the Radiating heat Unit was instead of a simulated heater. The boundaries were based on the thermal interface condition with the lunar lander, which varies from −110°C~ + 110°C. The thermal test verified the capability of the EUV camera to operate satisfactorily in vacuum at the expected hot and cold temperatures and the survival in non-operational extreme conditions without degradation of functional performance. The position pointing performance doesn't be changed significantly after thermal cycles, maintaining 2′ position accuracy. The minimum torque of moving the 2-axis mechanism smoothly were evaluated under hot and cold condition according to the operation voltage of stepper motor, the driving torque of 50mN·m demonstrate it has proper safety margin under the lunar enter.

For optical performance testing [14,15], since the size of the illuminated beam at 30.4nm from the monochromator is small, the EUV camera have to be rotated about the elevation axis and azimuth axis at different angle to obtain the image at different position in the field of view. The resolution target USA1951 was set at the focal plane of the collimator, the angle resolution of the EUVC can be calculated by the follow equation:

$$\alpha = \arg tg \frac{1}{2 \cdot \nu \cdot f_c} \tag{1}$$

#210949 - $15.00 USD Received 5 May 2014; revised 29 May 2014; accepted 16 Jun 2014; published 20 Jun 2014

ν—the frequency of the minimum pair of lines recognized by eyes;

f_c—the focal length of the collimator;

The beam magnified image recorded on the detector demonstrate that the EUVC can distinguish 0.2mm line width, so corresponding the 148mm effective focal length, the angle resolution is 0.08°,less than the design value of 0.1°. Although the resolution of full aperture can't be determined directly by imaging a narrow collimated beam, the image quality (photometry, linearity), noise evaluation of the whole instrument could be verified based on the response model of MCP detector and electronic subsystem which have been calibrated in vacuum test facility. The end-to-end measuring results before launching are shown in Fig. 6.

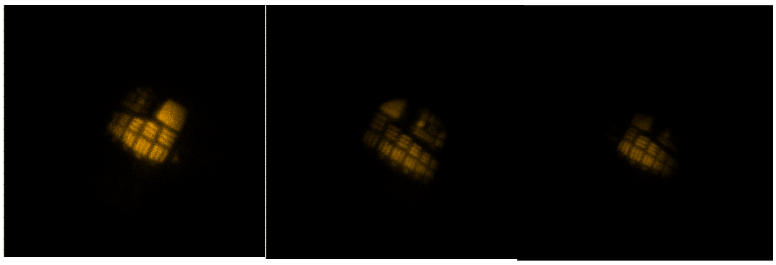

Fig. 6. Narrow beam image at detector for different incident angle.

The field-dependent distortion of the image was measured in 5 locations of the pupil, then adjust the position coefficients of three readout circuits from MCP detector to enable the EUVC to image uniformity. Figure 7 shows the comparison of image before and after correction, the results indicate the end-to-end characteristics of the full instrument is in the expected state by design.

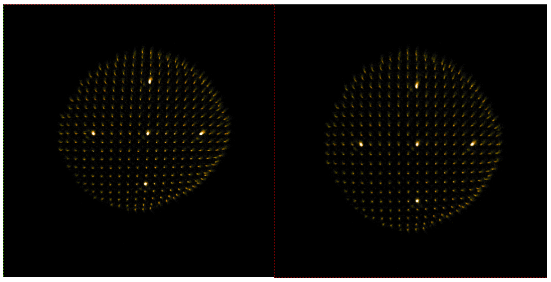

Fig. 7. Spot distortion at the different location of the detector.

8. Conclusions

The opto-mechanical design of EUVC has fully taken into accounting the primary limiting conditions, such as wide ranges of temperature change, severe vibration and shock, strict requirements of weight and volume and so on, and finally achieved the design optimization and design goal of EUVC on a lightweight, compact, high rigidity and stability.

The EUVC has been extensively tested in the qualification and verification test program. The vibration test shows the adequate eigenfrequencies and gives evidence on the integrity of the mechanical design in terms of stiffness and strength. Elevation drive module and azimuth drive module of the 2-axis platform, as well as the aperture door mechanism adopted the same kind of drive manner: worm-wheel and step motor, so it is relatively easy to control the dynamic characteristics of the 2-axis platform including reliability and stability of movement in the required environmental conditions, the pointing performance and the safety margin of driving torque have been checked and they were in accord with expectations. The image performance test indicated that the image angle resolution is less than 0.1°, the distortion and

#210949 - $15.00 USD Received 5 May 2014; revised 29 May 2014; accepted 16 Jun 2014; published 20 Jun 2014

dark calculation level is in the tolerance range. In general, the design, and assembly and tests successfully satisfy the lunar landing mission requirements.

Acknowledgments

We acknowledge with appreciation the cooperation and support of the Center of Chinese Space Science throughout the EUVC development. We wish to acknowledge Professor Jingjiang Xie in the Center of Optics Technique in Changchun Institute of Optics, Fine mechanics and Physics who made the super smooth mirror for the project.

#210949 - $15.00 USD Received 5 May 2014; revised 29 May 2014; accepted 16 Jun 2014; published 20 Jun 2014